



# eWaSR – an embedded-compute-ready maritime obstacle detection network

Matija Teršek <sup>1,2</sup> , Lojze Žust <sup>2</sup> , Matej Kristan <sup>2</sup> 

<sup>1</sup> Luxonis Holding Corporation

<sup>2</sup> Faculty of Computer and Information Science, University of Ljubljana, Večna pot 113, 1000 Ljubljana, Slovenia

\* Correspondence: matija@luxonis.com

**Abstract:** Maritime obstacle detection is critical for safe navigation of autonomous surface vehicles (ASVs). While the accuracy of image-based detection methods has advanced substantially, their computational and memory requirements prohibit deployment on embedded devices. In this paper we analyze the currently best-performing maritime obstacle detection network WaSR. Based on the analysis we then propose replacements for the most computationally intensive stages and propose its embedded-compute-ready variant eWaSR. In particular, the new design follows the most recent advancements of transformer-based lightweight networks. eWaSR achieves comparable detection results to state-of-the-art WaSR with only 0.52% F1 score performance drop and outperforms other state-of-the-art embedded-ready architectures by over 9.74% in F1 score. On a standard GPU, eWaSR runs 10× faster than the original WaSR (115 FPS vs 11 FPS). Tests on a real embedded device OAK-D show that, while WaSR cannot run due to memory restrictions, eWaSR runs comfortably at 5.5 FPS. This makes eWaSR the first practical embedded-compute-ready maritime obstacle detection network. The source code and trained eWaSR models are publicly available here: <https://github.com/tersekmatija/eWaSR>.

**Keywords:** maritime obstacle detection, semantic segmentation, efficient architecture, light-weight neural network, embedded hardware, OAK-D.

## 1. Introduction

Autonomous surface vehicles (ASVs) are emerging machines, catering a range of applications such as monitoring of the aquatic environment, inspection of hazardous areas, and automated search-and-rescue missions. Considering they do not require a crew, they can be substantially downsized and thus offer potentially low operating costs. Among other capabilities, reliable obstacle detection plays a crucial role in their autonomy, since timely detection is required to prevent collisions which could damage the vessel or cause injuries.

The current state-of-the-art (SOTA) algorithms for maritime obstacle detection [1] are based on semantic segmentation and classify each pixel of the input image as an obstacle, water, or sky. These models excel at detecting static and dynamic obstacles of various shapes and sizes, including those not seen during training. Additionally, they provide a high degree of adaptability to challenging and dynamic water features for successful prediction of the area that is safe to navigate. However, these benefits come at a high computational cost, as most of the recent SOTA semantic segmentation algorithms for maritime [1–3] and other [4,5] environments utilize computationally-intensive architectural components with a large number of parameters and operations. SOTA algorithms therefore typically require expensive and energy-inefficient high-end GPUs, making them unsuitable for real-world small energy-constrained ASVs.

Various hardware designs have been considered to bring neural network inference to industry applications. These include edge TPUs [6], embedded GPUs [7], and dedicated hardware accelerators for neural network inference [8]. In this paper, we consider OAK-D [9], a smart stereo camera which integrates the MyriadX VPU [8]. OAK-D reserves 1.4 TOPS for neural network inference and contains 385.82 MiB on-board memory for neural networks,



**Citation:** Teršek, M.; Žust, L.; Kristan, M. eWaSR – an embedded-compute-ready maritime obstacle detection network. *Preprints* 2023, 1, 0. <https://doi.org/>

**Publisher's Note:** MDPI stays neutral with regard to jurisdictional claims in published maps and institutional affiliations.



**Copyright:** © 2023 by the authors. Licensee MDPI, Basel, Switzerland. This article is an open access article distributed under the terms and conditions of the Creative Commons Attribution (CC BY) license (<https://creativecommons.org/licenses/by/4.0/>).

programs, stereo depth computation, and other image-manipulation-related operations. These properties make it an ideal embedded low-power smart sensor for autonomous systems such as ASVs.

However, state-of-the-art models, such as WaSR [1], cannot be deployed to OAK-D due to memory limitations, and many standard models that can be deployed, such as U-Net [4], typically run at less than 1 FPS, which is impractical. These limitations generally hold for other embedded devices as well. Recent works [3,10] consequently explored low-latency light-weight architectures for ASVs, but their high throughput comes at a cost of reduced accuracy. While significant research has been invested in development of general embedded-ready backbones [11–18], these have not yet been analyzed in the aquatic domain and generally also sacrifice accuracy in our experience. For these reasons there is a pressing need for ASV obstacle detection embedded-compute-ready architectures, that do not substantially compromise the detection accuracy.

To address the aforementioned problems, we propose a fast and robust neural network architecture for ASV obstacle detection, capable of low latency on embedded hardware with a minimal accuracy trade-off. The architecture, which is our main contribution, is inspired by the current state-of-the-art WaSR [1], hence the name *embedded-compute-ready WaSR* (eWaSR). By careful analysis we identify the most computationally intensive modules in WaSR and propose computationally efficient replacements. We further reformulate WaSR in the context of transformer-based architectures and propose Channel Refinement Module (CRM) and Spatial Refinement Module (SRM) blocks for efficient extraction of semantic information from images features. On a standard GPU, eWaSR runs at 115 FPS, which is  $10\times$  faster than the original WaSR [1], with an on-par detection accuracy. We also deploy eWaSR on a real embedded device OAK-D, where it comfortably runs at 5.5 FPS, in contrast to the original WaSR, which cannot even be deployed on the embedded device. The source code and trained eWaSR models are publicly available<sup>1</sup> to facilitate further research in embedded maritime obstacle detection.

The remainder of the paper is structured as follows: Section 2 reviews the existing architectures for maritime obstacle detection, efficient encoders, and light-weight semantic segmentation architectures. Section 3 analyzes the WaSR [1] blocks, their importance, and bottlenecks. The new eWaSR is presented in Section 4 and extensively analyzed in Section 5. Finally, the conclusions and outlook are drawn in Section 6.

## 2. Related work

### 2.1. Maritime obstacle detection

Classical maritime obstacle detection methods can be roughly split into detector-based methods (using Viola & Jones [19], Haar [20], or HOG [21]), segmentation-based methods (Markov random fields [22] or background subtraction [23]), and saliency map methods [24]. These methods rely on simple hand-crafted features, which are not expressive enough for accurate detection in challenging environments. Convolutional neural networks (CNN) overcome this limitation, and are widely adopted in modern methods. Several detector-based methods have been explored. Lee *et al.* [25] uses transfer learning on YoloV2 [26] and fine-tunes it on the SMD [27] dataset for obstacle detection. Yang *et al.* [28] uses a deep convolutional network and a Kalman filter for high-performance object detection and tracking. Ma *et al.* [29] replaces the backbone in Faster R-CNN [30] with ResNet [31], and improves the detection by combining multi-layer detail features and high-level semantic features with a modified DenseNet block [32].

Despite the remarkable progress of CNN-based object detection, these models do not generalize well to previously unseen obstacles and cannot address static obstacles such as piers

<sup>1</sup> <https://github.com/tersekatija/eWaSR>

and shorelines. For this reason, the most successful techniques adopt the principle originally proposed by Kristan *et al.* [22], which employs semantic segmentation to determine image regions corresponding to water (i.e., are safe to navigate) and regions corresponding to non-navigable area (i.e., obstacles). Cane and Ferryman [33] evaluated three semantic segmentation architectures (SegNet [34], ENet [35], ESPNet [36]) in a maritime environment and found that while the models perform well in urban scenarios, they suffer from a high false positive rate due to reflections, glare, wakes, and challenging water shape. Bovcon *et al.* [37] made the same observation and proposed the first maritime obstacle detection per-pixel annotated training dataset MaSTr1325 to facilitate development of maritime-specific segmentation-based architectures. Their analysis of standard architectures (U-Net [4], PSPNet [38], and DeepLabV2 [5]) pointed out that foam, glitter, and mirroring appear to be major contributors to detection failure.

In response to findings of [33,37], Bovcon and Kristan [1] proposed an encoder-decoder architecture WaSR based on DeepLabv2 [5] with additional blocks inspired by BiSeNet [39]. With a carefully designed decoder and a novel water-obstacle separation loss on encoder features, the model can learn dynamic water features, perform better than existing algorithms under reflections and glare, and achieve state-of-the-art results. According to the major maritime obstacle detection benchmark [40] WaSR remains the current state-of-the-art. Žust and Kristan [2] upgraded this architecture by a temporal context module that extracts spatio-temporal texture to cope with reflections. While achieving impressive results, all top-performing maritime obstacle detection methods require powerful GPUs, making them unsuitable for small-sized ASVs with limited computational and energy resources.

## 2.2. Efficient neural networks

Several works consider the general problem of efficient light-weight architectures that can run on low-power devices. GhostNet [13] applies low-cost linear operations to generate various feature maps, with the goal of revealing information of underlying intrinsic features at a lower cost. MobileNets [11,12,41] factorize convolutions into depthwise and pointwise convolutions, propose a hard swish activation function, Squeeze-and-Excite [42] blocks, and neural architecture search (NAS) to find the best architectures for mobile CPUs. ShuffleNet [14,43] introduces channel shuffling to simplify and speed-up pointwise convolutions. EfficientNets [44,45] scale the width, depth, and resolution of architectures to achieve various accuracy and latency trade-offs. RegNets [15] define convolutional network design space that provides simple and fast networks under various regimes. MicroNets [16] integrate sparse connectivity and propose novel activation functions to improve nonlinearity in low-parameter regimes. RepVGG [17] utilizes structural reparameterization to transform a multi-branch architecture during training into a plain VGG-like [46] architecture at inference time with minimal memory access. MobileOne [18] extends the idea by introducing trivial over-parameterization branches and replacing convolutions with depthwise and pointwise convolutions. The re-parameterization trick makes RepVGG and MobileOne suitable for embedded devices as they achieve good accuracy at reduced latency compared to the other state-of-the-art encoder architectures, despite having more parameters and FLOPs. Metaformer [47] abstracts the transformer architecture and shows that costly attention can be replaced by a simple operation such as pooling, without substantially hampering the performance.

Several optimizations to improve and speed-up networks for the task of semantic segmentation have also been proposed. ICNet [48] uses a cascade feature-fusion unit that combines semantic information from low resolution and details from high resolution. ESPNet [36] learns the representations from a larger receptive field by using a spatial pyramid with dilated convolutions in a novel efficient spatial pyramid (ESP) convolutional module. BiSeNet [39] introduces separate spatial and semantic paths and blocks for feature fusion and channel

attention to efficiently combine features from both paths in order not to compromise the spatial resolution while achieving faster inference. SwiftNet [49] triggers memory updates on parts of frames with higher inter-frame variations to compress spatio-temporal redundancy and reduce redundant computations. The recently proposed TopFormer [50] uses convolutional neural networks to extract features at different scales and efficiently extracts scale-aware semantic information with consecutive transformer blocks at low resolution. Those are later fused in a simple but fast novel semantic injection module, reducing the inference time.

### 3. WaSR architecture analysis

An important drawback of the currently best-performing maritime obstacle detection network WaSR [1] are its computational and memory requirements that prohibit application on low-power embedded devices. In this section we therefore analyze the main computational blocks of WaSR in terms of resource consumption and detection accuracy. These results are the basis of the new architecture proposed in Section 4.

The WaSR architecture, summarized in Figure 1, contains three computational stages: the encoder, a feature mixer, and the decoder. The encoder is a ResNet-101 [31] backbone, while the feature mixer and decoder are composed of several information fusion and feature scaling blocks. The first fusion block is called *channel attention refinement module* (cARM1 and cARM2 in Figure 1) [39], which reweights the channels of input features based on the channel content. The per-channel weights are computed by averaging the input features across spatial dimensions, resulting in a  $1 \times 1$  feature vector that is passed through a  $1 \times 1$  convolution followed by a sigmoid activation. The second fusion block is called a *feature fusion module* (FFM) [39], which fuses features from different branches of the network by concatenating them, applying a  $3 \times 3$  convolution and a channel reweighting technique similar to cARM1 with  $1 \times 1$  convolutions and a sigmoid activation. The third major block is called *trous spatial pyramid pooling* (ASPP) [5], which applies convolutions with different dilation rates in parallel and merges the resulting representations to capture object and image context at various scales. The feature mixer and the decoder also utilize the Inertial Measurement Unit (IMU) sensor readings in the form of a binary encoded mask that denotes horizon location at different fusion stages. In addition to the focal loss  $\mathcal{L}_{\text{foc}}$  [51] for learning semantic segmentation from ground-truth labels, Bovcon and Kristan [1] proposed a novel water-obstacle separation loss  $\mathcal{L}_{R1}^{R2}$  to encourage the separation of water and obstacle pixels in the encoder’s representation space.

We note that the encoder is the major culprit in memory consumption, since it employs the ResNet-101 [31] backbone. This can be trivially addressed by replacing it by any light-weight backbone. For example, replacing the backbone with ResNet-18, which uses approximately  $4 \times$  less parameters and  $18 \times$  less FLOPs than ResNet-101 (11.7M and 7.2G vs. 44.5M and 133.8G), and does not use dilated convolutions, thus producing smaller feature maps, already leads to a variant of WaSR that runs on an embedded device. Concretely, a WaSR variant with a ResNet-18 encoder runs at 5.2 FPS on OAK-D, but suffers in detection accuracy (a 0.90% F1 drop overall and 10.79% F1 drop on close obstacles in Section 5). The performance will obviously depend on the particular backbone used and we defer the reader to Section 5, which explores various light-weight backbone replacements.

We now turn to analysis of the WaSR computational blocks in feature mixer and decoder. The detection performance contribution of each block is first analyzed by replacing it with a  $1 \times 1$  convolution and retraining the network (see Section 5 for the evaluation setup). Results in Table 1 indicate a substantial performance drop of each replacement, which means that all blocks indeed contribute to the performance and cannot be trivially avoided for speedup. Table 2 reports the computational requirements of each block in terms of the number of parameters, floating point operations (FLOPs), and the execution time of each block measured by the

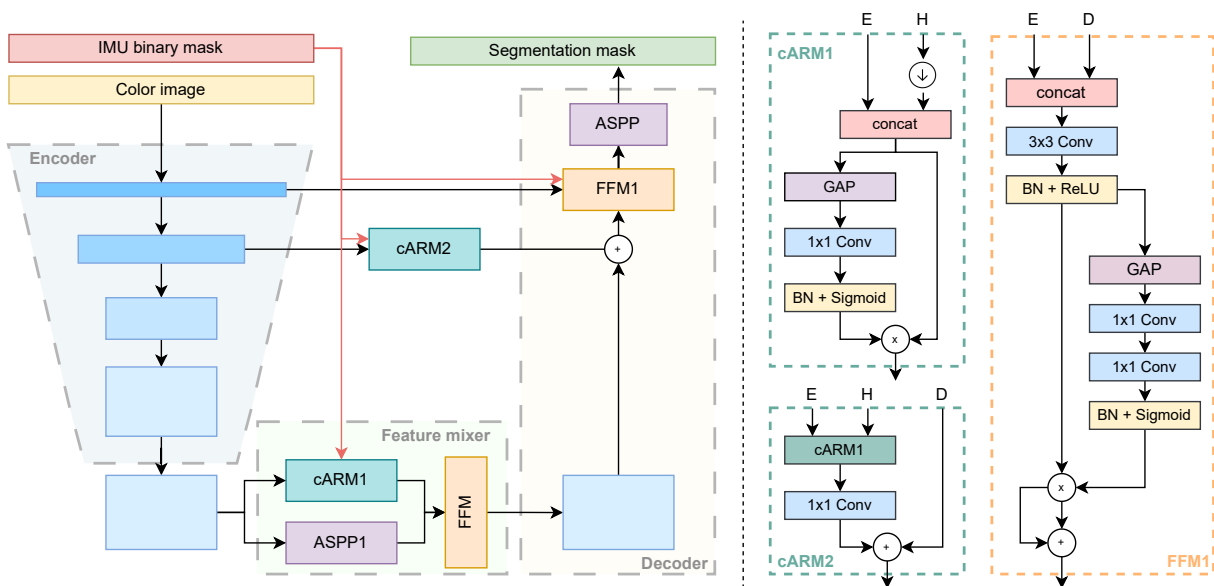


**Figure 1.** The WaSR [1] architecture (left), and the FFM1, cARM1, and cARM2 blocks (right) – the FFM block is same as FFM1, except it takes as the input the encoder features, the downsampled IMU and the upsampled decoder features.  $\downarrow$  stands for downsampling, E stands for encoder features, D for decoder features, and H for binary IMU mask (horizon) features.

**Table 1.** Overall F1 score of WaSR and its modifications by replacing each block by a  $1 \times 1$  convolution. The blocks corresponding to feature mixer are denoted by light gray.

WaSR	Original	-ASPP1	-cARM1	-FFM	-cARM2	-ASPP	-FFM1
<b>F1</b>	93.5%	-0.8%	-0.8%	-1.2%	-1.0%	-1.4%	-0.7%

PyTorch Profiler<sup>2</sup> on a modern laptop CPU. Results indicate that the FFM and FFM1 blocks are by far the most computationally intensive. The reason lies in the first convolution block at the beginning of the FFM block (Figure 1), which mixes a large number of input channels, thus entailing a substantial computational overhead. For example, the first convolution in each FFM block accounts for over 90% of the block execution time. In comparison, ASPP is significantly less computationally intensive and cARM is the least demanding block.

Both, FFM and cARM blocks contain a channel re-weighting branch, which entails some computational overhead. We therefore inspect the diversity level of the computed per-channel weights as an indicator of re-weighting efficiency. The weight diversity can be quantified by per-channel standard deviations of the predicted weights across several input images. Figure 2 shows the distribution of the standard deviations computed on the MaStr1325 [37] training set images for FFM and cARM blocks. We observe that the standard deviations for FFM blocks are closer to 0 compared to cARM1 and have a shorter right tail compared to cARM2. This suggests that the per-channel computed weights in FFM/FFM1 blocks do not vary much across the images, thus a less computationally-intensive replacements could be considered. On the other hand, this is not true for the cARM blocks, where it appears that the re-weighting changes substantially across the images. A further investigation of the cARM blocks (see supplementary material in Appendix A) shows that the blocks learn to assign a higher weight to the IMU

<sup>2</sup> <https://pytorch.org/docs/stable/profiler.html>

**Table 2.** WaSR decoder computational analysis in terms of number of parameters (in millions), FLOPs (in billions), and the PyTorch profiler output (the total execution time of each block as well as the execution of the slowest operation in the block – Max execution) on the CPU. The blocks corresponding to feature mixer are denoted by light gray.

Block	Parameters (M)	FLOPs (B)	Total execution time [ms]	Max execution time [ms]
ASPP1	1.77	5.436	48.83	18.06
cARM1	4.20	0.0105	12.36	3.99
FFM	<b>21.28</b>	<b>58.928</b>	<b>279.40</b>	<b>266.32</b>
cARM2	0.79	1.617	19.81	10.54
ASPP	0.11	1.359	66.75	17.16
FFM1	<b>13.91</b>	<b>145.121</b>	<b>641.23</b>	<b>589.55</b>

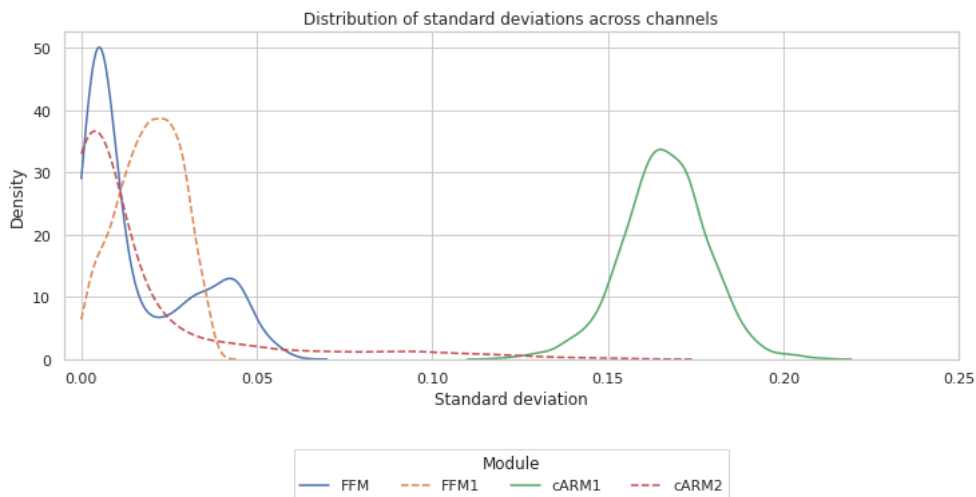


**Figure 2.** Distribution of per-channel standard deviations of channel re-weighting sigmoid activations across images of the MaSTr1325 training set in the cARM and FFM blocks. Lower standard deviation indicates that channels are given a similar weight in each image.

channel in images where horizon is poorly visible. This further indicates the utility of the cARM blocks.

In terms of the WaSR computational stages, Table 2 indicates that the decoder stage entails nearly twice as much total execution time compared to the feature mixer stage. Nevertheless, since the computationally-intensive blocks occur in both stages, they are both candidates for potential speedups by architectural changes.

#### 4. Embedded-compute-ready obstacle detection network eWaSR

The analysis in Section 3 identified the decoder as the most computationally- and memory-hungry part of WaSR, with the second most intensive stage being the backbone. As noted, the backbone can be easily sped up by considering a light-weight drop-in replacement. However, this leads to detection accuracy reduction due to semantically impoverished backbone features. Recently, Zhang *et al.* [50] proposed compensating for semantic impoverishment of light-weight backbones by concatenating features at several layers and mixing them using a transformer. We follow this line of architecture design in eWaSR, shown in Figure 3.

We replace the ResNet-101 backbone in WaSR by a light-weight counterpart ResNet-18 and concatenate the features from the last layer with resized features from layers 6, 10, and 14.



These features are then semantically enriched by the feature mixer stage. The recent work [50] proposed a transformer-based mixer capable of producing semantically rich features at low computational cost. However, the transformer applies token cross-attention [52], which still adds a computationally prohibitive overhead. We propose a more efficient feature mixer that draws on findings of Yu *et al.* [47] that computationally-costly token cross-attentions in transformers can be replaced by alternative operations, as long as they implement cross-token information flow.

We thus propose a Light-weight Scale-Aware Semantic Extractor (LSSE) for the eWaSR feature mixer, which is composed of two metaformer refinement modules CRM and SRM (Figure 3). Both modules follow the metaformer [47] structure and differ in the type of information flow implemented by the token mixer. The channel refinement module (CRM) applies the cARM [39] module to enable a global cross-channel information flow. This is followed by a spatial refinement module (SRM), which applies sARM [53] to enable cross-channel spatial information flow. To make the LSSE suitable for our target hardware, we replace the commonly-used GeLU and layer normalization blocks of metaformer by ReLU and batch normalization. The proposed LSSE is much more computationally efficient than SSE [50]. For example, with a ResNet-18 encoder, the SSE would contain 66.4M parameters (requires 3.2GFlops), while the LSSE contains 47.9M parameters (requires 2.1GFlops).

We also simplify the WaSR decoder following the TopFormer [50] semantic-enrichment routines to avoid the computationally-costly FFM and ASPP modules. In particular, the output features of the LSSE module are gradually upsampled and fused with the intermediate backbone features using the semantic injection modules [50] (SIM). To better cope with the maritime dynamic environment and small objects, the intermediate backbone features on the penultimate SIM connection are processed by two SRM blocks. The final per-layer semantically enriched features are concatenated with the IMU mask and processed by a shallow prediction head to predict the final segmentation mask. The prediction head is composed of a  $1 \times 1$  convolutional block, a batchnorm and ReLU, followed by  $1 \times 1$  convolutional block and softmax.

## 5. Results

### 5.1. Implementation details

eWaSR employs the same losses as WaSR [1]: Focal loss [51] is applied on segmentation along with  $L_2$  weight decay regularizer [54] and the water-obstacle separation loss [1] is applied to the backbone features (layer 14 in ResNet-18) to encourage learning embedding with well separated water and obstacle features. Network training follows the procedure in [1]. We train for 100 epochs with the patience of 20 epochs on validation loss, RMSProp optimizer with 0.9 momentum, and learning rates of  $10^{-6}$  and  $10^{-5}$  for backbone and decoder, respectively. Contrary to WaSR [1], we train eWaSR and other networks that rely on metaformers with a batch size 16 and a maximum of 200 epochs, since transformers benefit from longer training on larger batches [55].

### 5.2. Training and evaluation hardware

All networks are trained on a single NVIDIA A4000 GPU. A laptop GPU NVIDIA RTX 3070Ti is used for GPU latency estimation, while the on-device performance tests are carried out on the embedded OAK-D [9] with 16 SHAVE cores, delivering 1.4 TOPS for on-device neural network inference. The power consumption of OAK-D is approximately 7.5W, which is far below 290W of the thermal design power (TDP) typical for user-grade GPUs such as Nvidia RTX 3070Ti, thus making it a suitable embedded device testing environment.

While OAK-D executes neural networks on-chip, it still requires a host machine (such as laptop or Raspberry Pi) that loads the pipeline with the models to the device. Because it is not

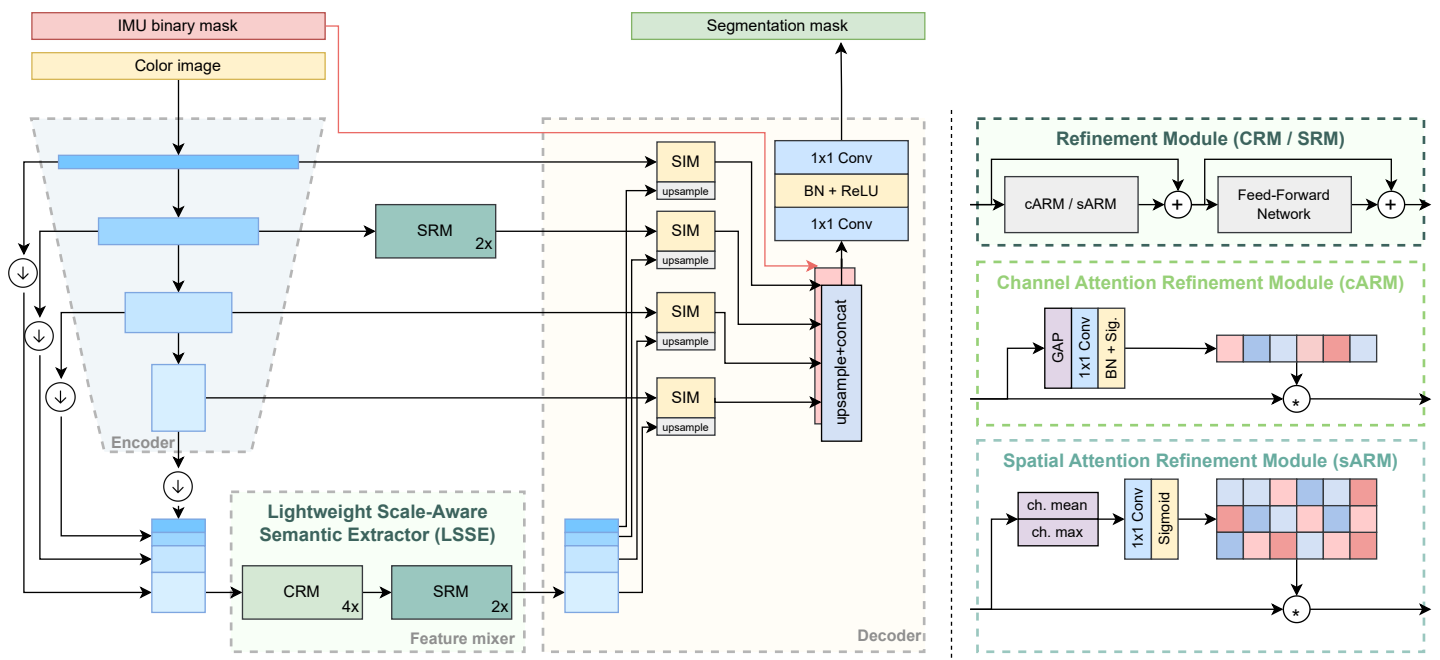


**Figure 3.** eWaSR architecture follows the encoder, feature mixer, and decoder architecture. The backbone features of intermediate encoder layers are resized, concatenated and processed by a light-weight scale-aware semantic extraction module (LSSE). The semantically-enriched features are injected into higher-layer backbone features by semantic-injection modules [50] SIM. The resulting features are then concatenated with the IMU mask and passed to the segmentation head.

possible to measure the raw inference time of the neural network execution, we measure the latency from the image sensor to receiving the output on the host computer. We reason that this is sufficient since this mimics the use of OAK-D in potential deployment, with inference being performed on OAK-D and the rest of navigation logic on the host machine. To reduce the effect of parallel execution, we allow only one image to be in the pipeline’s queue and use a single neural network processing thread when measuring the latency. The latency is thus estimated as the time between the outputs, averaged over 200 outputs. We use both inference threads when reporting FPS.

### 5.3. Datasets

All architectures are trained on Maritime Semantic Segmentation Training Dataset (MaSTr1325) [37], which contains 1325 per-pixel annotated images captured by an ASV. The images contain various obstacles of different sizes and shapes, such as swimmers, buoys, seagulls, ships, and piers, and are captured in different weather conditions. The pixels are annotated as either obstacle, sky, water, or unknown/ignore class. Each image is accompanied by a binary IMU mask, which is obtained by transforming the IMU readings into a horizon position in the image and setting all pixels above the horizon to 1 and the rest to zero.

The networks are evaluated on the recently proposed MODS [40] benchmark using their standard evaluation protocol. The dataset consists of 94 sequences with approximately 8000 annotated images collected with an ASV. Each frame is accompanied by the IMU mask. Unlike MaSTr1325, MODS does not include per-pixel labels and is instead designed with simpler annotations to evaluate models in two important aspects for ASV navigation – water-edge estimation and obstacle detection. Water-edge estimation measures the accuracy of water-land boundary predictions as a root mean squared error (RMSE) between the predicted water



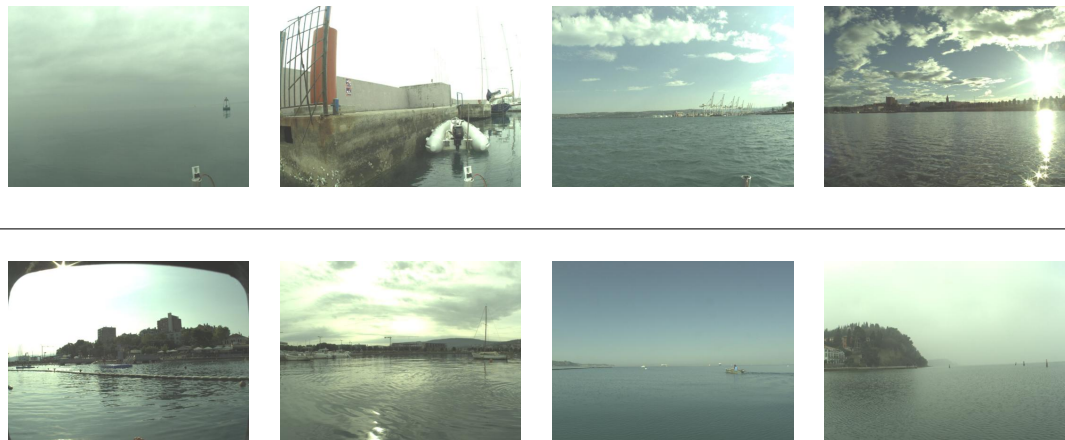


**Figure 4.** Example images from MaSTr1325 [37] dataset (top) and MODS [40] benchmark (bottom). Both datasets include challenging scenarios with varied obstacles and diverse weather conditions.

boundary and the ground truth annotations (water-edge polyline). Ground-truth dynamic obstacles are annotated as bounding boxes. To measure the obstacle detection performance, a prediction is considered as a true positive (TP) if a sufficient area of the GT bounding box is covered with an obstacle mask. If this condition is not met, the GT obstacle is considered a false negative (FN). Blobs predicted as obstacles in the water regions outside the GT bounding boxes are considered false positives (FP). The obstacle detection task is finally summarized by precision ( $Pr = \frac{TP}{TP+FP}$ ), recall ( $Re = \frac{TP}{TP+FN}$ ), and F1 ( $= \frac{2 \cdot Pr \cdot Re}{Pr+Re}$ ) score, and is evaluated for all obstacles in the image (reported as Overall) and obstacles at the maximum distance of 15 meters from the vessel (reported as Danger Zone), which pose an immediate threat to the vehicle. In this paper, we report the performance of both aspects of MODS, but put more focus on the obstacle detection aspect as it is more important for the safe navigation of ASVs. Examples of images from the MaSTr1325 and MODS datasets are shown in Figure 4.

#### 5.4. Influence of light-weight backbones on WaSR performance

As noted in Section 3, WaSR [1] can be trivially modified to run on embedded device by replacing its Reset-101 backbone with a light-weight counterpart. We explore here several alternatives to arrive at a strong baseline. In particular, the following eight light-weight backbones are considered: ResNet-18 [31], RepVGG-A0 [17], MobileOne-S0 [18], MobileNetV2 [12], GhostNet [13], MicroNet [16], RegNetX [15], and ShuffleNet [43]. The backbone implementations are based on official ([13,16–18]) and torchvision [56] implementations.

Table 3 reports the obstacle detection performance, the inference times on GPU and OAK-D, and the combined number of channels in the intermediate multi-scale features of the encoder for several light-weight backbones. The WaSR variant with a ResNet-18 [31] backbone achieves the highest F1 score overall (92.56%), while the model with a RegNetX [15] encoder performs the best inside the danger zone (83.95% F1) at the cost of being the slowest on OAK-D (395.22 ms). In contrast, MicroNet-M0 is the fastest on OAK-D (75.0 ms) but achieves the lowest overall F1 score (68.49%). GhostNet [13] is the fastest on the GPU (5.55 ms). In addition to GhostNet, the latency of MicroNet-M0 [16], GhostNet, and MobileNetV2 [12] is also below 150 ms and 6 ms on OAK-D and GPU, respectively. All three models have less than 472 total channels, followed by ResNet-18 encoder with 960 channels. Despite having a larger total number of channels from the intermediate features, RepVGG [17] and MobileOne [18] achieve a similar overall (91.81% and 91.25%) and better danger zone F1 scores (80.73% and 82.41%) than the ResNet-18 model (92.56% overall F1, 78.09% danger zone F1), with a lower latency (225.02

**Table 3.** Light-weight WaSR variants with different backbones comparison in terms of water-edge accuracy, overall and danger zone F1 score, the latency on OAK-D and GPU, and the total number of channels of the multi-scale encoder. Gray highlight denotes our chosen baseline model WaSR-Light and the best results for each metric are denoted in bold.

encoder	W-E	Overall			Danger zone (< 15m)			Latency		
		Pr	Re	F1	Pr	Re	F1	OAK	GPU	chs
ResNet-18 [31]	20px	93.46	91.67	<b>92.56</b>	66.98	93.61	78.09	314.64	7.66	960
RepVGG-A0 [17]	19px	91.71	91.9	91.81	70.49	94.44	80.73	225.02	6.06	1616
MobileOne-S0 [18]	18px	92.2	90.33	91.25	73.59	93.64	82.41	283.89	6.47	1456
MobileNetV2 [12]	24px	90.05	85.99	87.98	63.71	91.69	75.18	149.97	5.66	472
GhostNet [13]	21px	90.47	89.72	90.1	59.4	92.96	72.49	129.81	<b>5.55</b>	<b>304</b>
MicroNet [16]	43px	63.59	74.22	<b>68.49</b>	15.28	71.8	25.19	<b>75.0</b>	5.60	436
RegNetX [15]	18px	91.89	89.55	90.7	76.75	92.65	<b>83.95</b>	395.22	9.80	1152
ShuffleNet [43]	23px	90.14	87.38	88.74	61.18	90.95	73.15	274.93	8.10	1192

and 283.89 ms, respectively, compared to 314.64 ms). The variant of WaSR with a ResNet-18 backbone achieves the best overall performance at low latency, which justifies it as a strong embedded-ready baseline and is referred to as *WaSR-Light* in the following analysis.

### 5.5. Comparison with the state of the art

We first compare our eWaSR with the baseline model WaSR-Light and the original WaSR [1]. Results are reported in Table 4. eWaSR most substantially outperforms WaSR-light inside the danger zone (+9.54% F1), which is the most critical for safe navigation. eWaSR is approximately 10% slower on GPU compared to the WaSR-Light (8.70 ms compared to 7.85 ms, respectively), but is approximately 5% faster on the embedded hardware (300.37 ms compared to 314.64 ms on OAK-D, respectively). The F1 performance of eWaSR is only slightly reduced compared to WaSR (−0.52% and −0.73% overall and inside the danger zone). Thus the detection performance of eWaSR is comparable with the original WaSR, while being over 10× faster on GPU (8.70 versus 90.91 milliseconds). Additionally, in contrast to WaSR, which cannot even be deployed on OAK-D due to memory constraints, eWaSR can comfortably run on-device at 5.45 FPS.

eWaSR is compared with 12 state-of-the-art or high-performing architectures designed for maritime or general semantic segmentation. Specifically, we evaluate the performance of BiSeNetV1<sub>MBNV2</sub> [12] [39], BiSeNetV2 [57], DDRNet23-Slim [58,59], EDANet [60], EdgeSegNet [61], LEDNet [62], MobileUNet [63], RegSeg [64], ShorelineNet [3], DeepLabV3<sub>MBNV2</sub> [12] [5], ENet [35], and Full-BN [10]. Table 4 shows that WaSR outperforms all these methods in the overall and danger-zone F1 score. It ranks 5<sup>th</sup> in latency on OAK-D, but outperforms all faster models by over 9.74% and 22.7% F1 overall and inside the danger zone, respectively. The excellent latency-performance trade-off of eWaSR is further confirmed in Figure 5.

Figure 6 shows qualitative comparison of eWaSR, WaSR-Light, and WaSR for further insights. We observe that eWaSR predicts fewer false positives in the presence of land and in the distance and predicts more accurate segmentation masks on distant vessels and their reflections. However, it similarly fails on large homogeneous surfaces. On the contrary, WaSR performs better in such cases, but predicts more false positives in presence of the piers. All models appear to experience false detections in some cases in the presence of wakes and glares, which is a point requiring further research in maritime obstacle detection.

**Table 4.** Comparison of the proposed eWaSR with state-of-the-art segmentation models and WaSR-Light. Best results are shown in bold, while (/) indicates that the model cannot be deployed on OAK-D due to unsupported operations or memory constraints.

Model	W-E	Overall			Danger zone (< 15m)			Latency	
		Pr	Re	F1	Pr	Re	F1	OAK	GPU
BiSeNetV1 <sub>MBNV2</sub> [12] [39]	46px	45.94	80.94	58.62	7.9	83.32	14.44	93.45	3.52
BiSeNetV2 [57]	36px	64.96	82.71	72.77	21.55	78.54	33.82	400.08	4.46
DDRNet23-Slim [58,59]	54px	74.82	74.24	74.53	35.5	75.08	48.21	<b>50.70</b>	<b>4.71</b>
EDANet [60]	34px	82.06	84.53	83.28	52.82	84.22	64.92	130.45	6.09
EdgeSegNet [61]	58px	75.49	85.39	80.13	27.48	82.33	41.21	570.52	11.36
LEDNet [62]	92px	74.64	80.46	77.44	24.33	73.01	36.5	306.25	9.48
MobileUNet [63]	47px	52.54	83.68	64.55	9.21	75.36	16.42	392.47	7.51
RegSeg [64]	54px	84.98	77.53	81.08	48.44	78.44	59.89	119.55	8.40
ShorelineNet [3]	19px	90.25	85.44	87.78	57.26	91.72	70.5	683.74	5.36
DeepLabV3 <sub>MBNV2</sub> [12] [5]	29px	90.95	80.62	85.47	82.54	86.84	84.64	308.42	14.71
ENet [35]	34px	46.12	83.24	59.35	7.08	78.07	12.98	/	7.52
Full-BN [10]	33px	71.79	85.34	77.98	20.43	84.53	32.91	649.96	11.37
TopFormer [50]	20px	93.72	90.82	92.25	75.53	94.38	83.91	608.32	9.53
WaSR [1]	18px	95.22	91.92	93.54	82.69	94.87	88.36	/	90.91
WaSR-Light (ours)	20px	93.46	91.67	92.56	66.98	93.61	78.09	314.64	7.85
eWaSR (ours)	<b>18px</b>	95.63	90.55	93.02	82.09	93.98	87.63	300.37	8.70

## 5.6. Ablation studies

### 5.6.1. Influence of backbones

As in the case of WaSR-Light, we analyze the impact of different light-weight backbones on eWaSR performance. Based on results from Table 3, we consider the backbones that do not reduce performance, or incur a minimal reduction, but also reduce the latency: RepVGG-A0 [17], MobileOne-S0 [18], RegNetX [15], MobileNetV2 [12] and GhostNet [13].

Results in Table 5 show that the fastest processing times are achieved by using GhostNet (OAK-D 174.97 ms) and MobileNetV2 (GPU 8.25 ms). However, this comes at a substantial danger-zone F1 score reduction compared to ResNet-18 (−17.88% and −8.48%, respectively). The latter achieves the best overall and danger zone F1 scores (93.02% and 87.63%, respectively), while still maintaining a good latency (300.37 ms on OAK-D). Contrary to the results in Table 3, MobileOne-S0 and RepVGG-A0 encoders produce a higher latency compared to eWaSR (388.44 ms and 374.95 ms, respectively) due to a high number of channels in the intermediate features (in total 1616, 1456, respectively, compared to 960 from ResNet-18). Consequently, FLOPs of eWaSR’s Light-weight Scale-Aware Semantic Extractor (LSSE) are 2.8× and 2.3× higher compared to LSSE in eWaSR with ResNet-18 encoder at no F1 improvement. This shows that while both, RepVGG-A0 and MobileOne-S0, reduce the latency at minimal accuracy cost in classification networks, they are not suitable for eWaSR or similar architectures operating on concatenated intermediate features. While eWaSR is not the fastest with ResNet-18 encoder, it outperforms other combinations by at least 0.17% overall F1 and 1.02% danger zone F1, while still maintaining a good latency (300.37 ms and 8.70 ms on OAK-D and GPU, respectively). Thus ResNet-18 is suggested as the primary backbone of eWaSR.

### 5.6.2. Token mixer analysis

To better understand the effect of spatial refinement in form of SRM for maritime obstacle detection in eWaSR, we perform two ablation studies. Table 6 shows that removing the proposed SRM on the penultimate SIM connection (Figure 3) results in a minimal overall performance drop (−0.08% F1), but the drop is particularly apparent within the danger zone

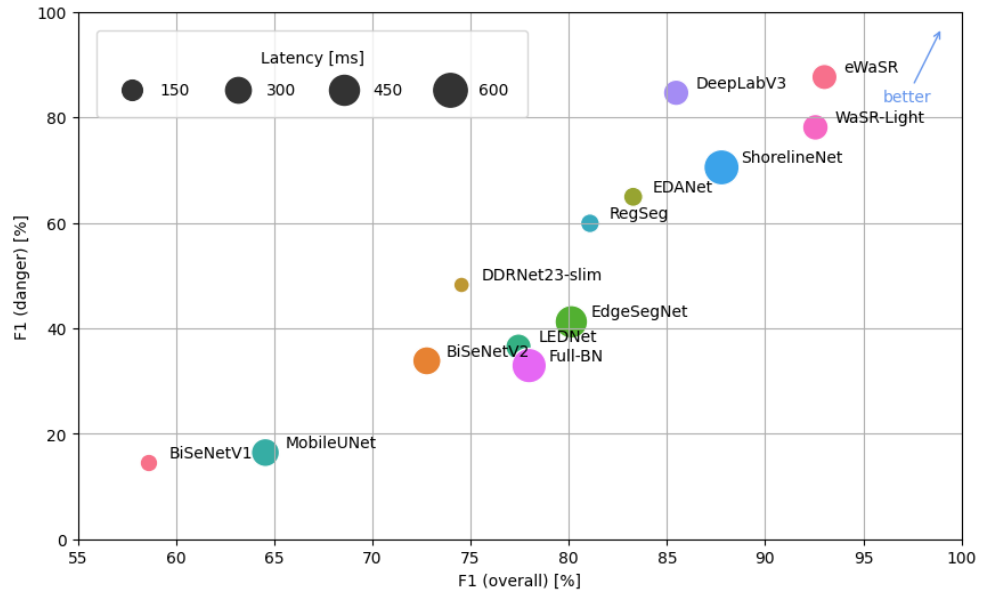


**Figure 5.** The latency-performance trade-off of the tested methods. Upper-right corner indicates top performance. eWaSR achieves the best overall and danger zone F1 score at a low latency on OAK-D.

**Table 5.** Detection accuracy and latency on OAK-D and GPU of eWaSR using different encoders. We see that the standard eWaSR with ResNet-18 encoder (highlighted in blue) achieves the best F1 score overall and inside the danger zone. In the last column, we show the total number of channels in concatenated features that are passed through LSSE. The best results are denoted in bold.

bb	W-E	Overall			Danger zone (< 15m)			Latency		
		Pr	Re	F1	Pr	Re	F1	OAK	GPU	chs
MobileOne-S0 [18]	20px	92.83	91.23	92.02	73.18	94.56	82.51	388.44	8.75	1456
RepVGG-A0 [17]	20px	95.33	90.49	92.85	80.1	94.26	86.61	374.95	9.92	1616
RegNetX [15]	21px	94.64	89.2	91.84	72.08	94.01	81.6	283.80	9.69	1152
MobileNetV2 [12]	21px	93.44	88.35	90.82	68.91	92.96	79.15	193.90	<b>8.25</b>	472
GhostNet [13]	23px	88.96	86.4	87.66	56.39	91.41	69.75	<b>174.97</b>	8.71	304
ResNet-18 [31]	<b>18px</b>	95.63	90.55	<b>93.02</b>	82.09	93.98	<b>87.63</b>	300.37	8.70	960

(−3.87% F1). Note that the removal does not substantially improve the inference time (−0.13 ms). The proposed spatial refinement module is thus crucial for improved detection accuracy of small objects, yet does not bring substantial computational overhead.

Next, we turn to the Light-weight Scale-Aware Semantic Extractor block, which also contains two SRM blocks. Table 6 shows that replacing these two with cARM-based CRM blocks results in a slight overall performance drop (−0.09% F1 compared to eWaSR), but a substantial drop inside the danger zone (−2.89% compared to eWaSR). While the latency is comparable, eWaSR works slightly faster than the variant with CRMs (−0.35 ms), since the convolutions in SRM operate on two channels only. The results thus confirm the performance benefits of SRM’s spatial refinement utilizing sARM in eWaSR.

### 5.6.3. Channel reduction speedup

As discussed in the beginning of the subsection, the results of Table 5 showed that the higher number of feature channels on skip connections connected to the decoder blocks increase the latency of eWaSR. We thus explore potential speedups by projection-based channel

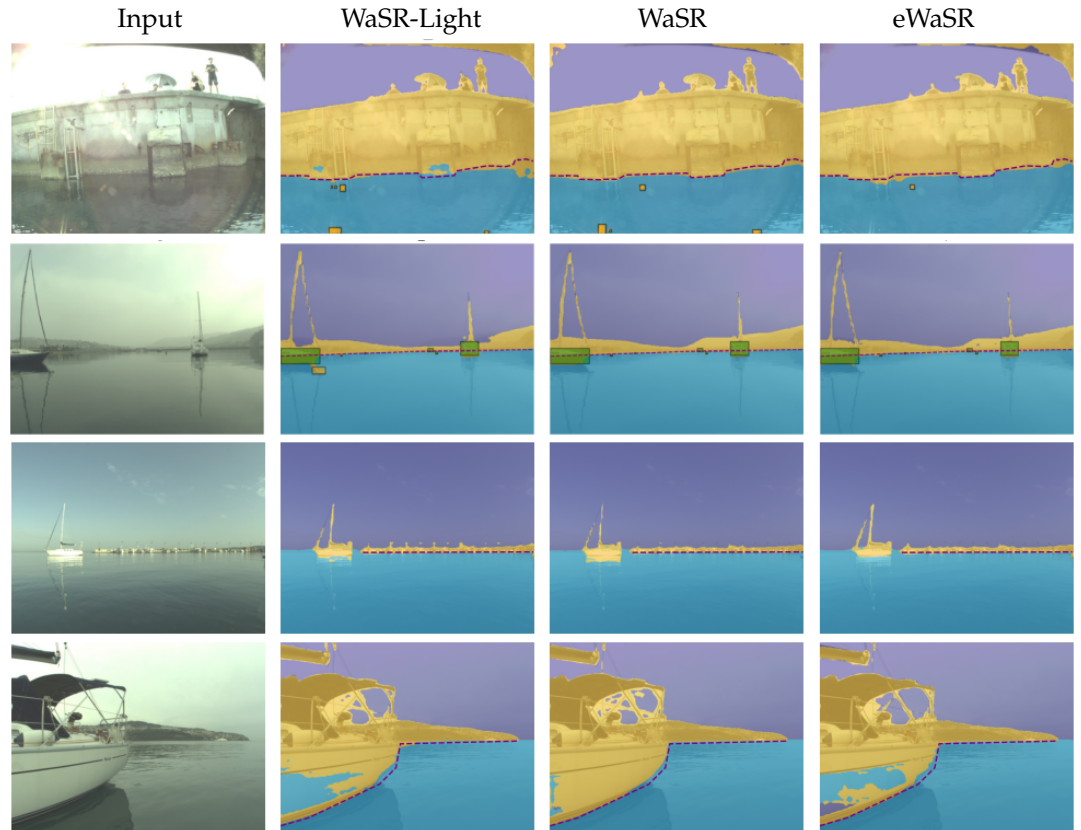


**Figure 6.** Results of eWaSR compared to baseline model WaSR-Light and WaSR. In the first column, we show an input image, followed by results of the baseline model, original WaSR model, and the proposed eWaSR. We can see that eWaSR has fewer FP predictions when close to piers (1<sup>st</sup> row) or in distance (2<sup>nd</sup> row). It can predict more refined segmentation masks than baseline in the distance (3<sup>rd</sup> row), but similarly struggles on flat surfaces of boats (4<sup>th</sup> row). We show TP (green) and FP (orange) bounding boxes in the first two rows, but omit them in the last two for better comparison.



**Table 6.** Results of ablation studies. We compare our proposed eWaSR (highlighted in blue) to modified eWaSR architecture without SRM on the penultimate SIM connection ( $\neg$ long-skip), without SRM in LSSE block ( $\neg$ SRM), and eWaSR with feature projection (reduction) on intermediate encoder outputs. We report overall and danger zone F1 on MODS [40] benchmark and latency on OAK-D and GPU.

modification	W-E	Overall	Danger	Latency	
		F1	F1	OAK	GPU
eWaSR	18px	<b>93.02</b>	<b>87.63</b>	300.37	8.70
$\neg$ long-skip	21px	92.94	83.76	300.24	8.68
$\neg$ SRM	19px	92.93	84.74	300.72	8.75
reduction	18px	92.39	85.81	<b>262.23</b>	<b>8.31</b>

reduction before concatenation of the encoder features into the LSSE and decoder, which maps all features to a lower dimension.

For easier comparison, we only focus on eWaSR with ResNet-18 encoder. Using  $1 \times 1$  convolution we halve the number of channels in each intermediate encoder output. As a result, the complexity of LSSE is noticeably decreased. In the case of ResNet-18 encoder, concatenated features only have 480 channels compared to 960 without projection. In Table 6 we compare the results of the model with projected features to eWaSR.

The model with projected features achieves slightly lower F1 scores ( $-0.63\%$  overall F1 and  $1.82\%$  danger zone F1, respectively) at approximately  $13\%$  speed-up (38.14 ms faster) on OAK-D, which means the projection trick is a viable option when one aims for a faster rather than a more accurate model and can be used in practical setups when a specific trade-off is sought in eWaSR performance.

## 6. Conclusion

We presented a novel semantic segmentation architecture for maritime obstacle detection eWaSR, suitable for deployment on embedded devices. eWaSR semantically enriches down-sampled features from ResNet-18 [31] encoder in a SSE-inspired [50] Light-weight Scale-Aware Semantic Extraction module (LSSE). We propose transformer-like blocks CRM and SRM, which utilize cARM [39] (channel-attention) and sARM [53] (simplified 2D spatial attention) blocks as token mixers, instead of costly transformer attention, and allow LSSE to efficiently produce semantically enriched features. Encoder features are fused with semantically enriched features in SIM [50] blocks. To help the model extract semantic information from a more detailed feature map, we use two SRM blocks on the second long skip connection, and we concatenate binary encoded IMU mask into the prediction head to inject information about tilt of the vehicle.

The proposed eWaSR is  $10\times$  faster than state-of-the-art WaSR [1] on a modern laptop GPU (8.70ms compared to 90.91ms latency, respectively) and can run comfortably at 5 FPS on embedded device OAK-D. Compared to other light-weight architectures for maritime obstacle detection [3,10], eWaSR does not sacrifice the detection performance to achieve the reduced latency, and achieves only  $0.52\%$  worse overall and  $0.73\%$  danger zone F1 score on the challenging MODS [40] benchmark compared to state-of-the-art.

Because of additional memory access, long-skip connections can increase the overall latency of the network. In the future, more emphasis could be put on exploring different embedded-compute suitable means of injecting detail-rich information to the decoder. While the goal of our work was to develop an efficient semantic segmentation network that can be deployed on embedded hardware, we did not consider the temporal component of the videos, which can boost the performance as shown in related work [2]. Furthermore, since OAK-D is



capable of on-board depth computation, fusion of depth into the model could be explored to increase the performance on close obstacles. We delegate this to the future work.

**Author Contributions:** Conceptualization, M.T. and M.K.; methodology, M.T. and M.K.; software, M.T. and L.Ž.; validation, M.T. and M.K.; formal analysis, M.T. and M.K.; data curation, M.T. and M.K.; writing, M.T., M.K. and L.Ž.; funding acquisition, M.K. All authors have read and agreed to the published version of the manuscript.

**Funding:** This research was funded by the Slovenian Research Agency program P2-0214 and project J2-2506.

**Institutional Review Board Statement:** Not applicable.

**Informed Consent Statement:** Not applicable.

**Data Availability Statement:** eWaSR: Code available at <https://github.com/tersekmatija/eWaSR> (accessed on 15 April 2023); MaStr1325: Publicly available at <https://www.vicos.si/resources/mastr1325/> (accessed on 22 January 2023); MODS: Publicly available at [https://github.com/bborja/mods\\_evaluation](https://github.com/bborja/mods_evaluation) (accessed on 22 January 2023).

**Conflicts of Interest:** The authors declare no conflict of interest.

## Appendix A. IMU channel weights in cARM blocks

Due to the architecture of the cARM block, we can directly look at the output of the sigmoid activation to obtain the weight for the IMU channel. In Figure A1 we show example images and corresponding IMU masks where the weight of the IMU channel is the lowest and the highest for both cARM blocks. We can see that where water and obstacle features are easier to separate, the IMU channel is given less weight. For images where the horizon is not clearly visible, either due to fog, bad weather, extreme glare, or exposure, the IMU channel is assigned a higher weight.

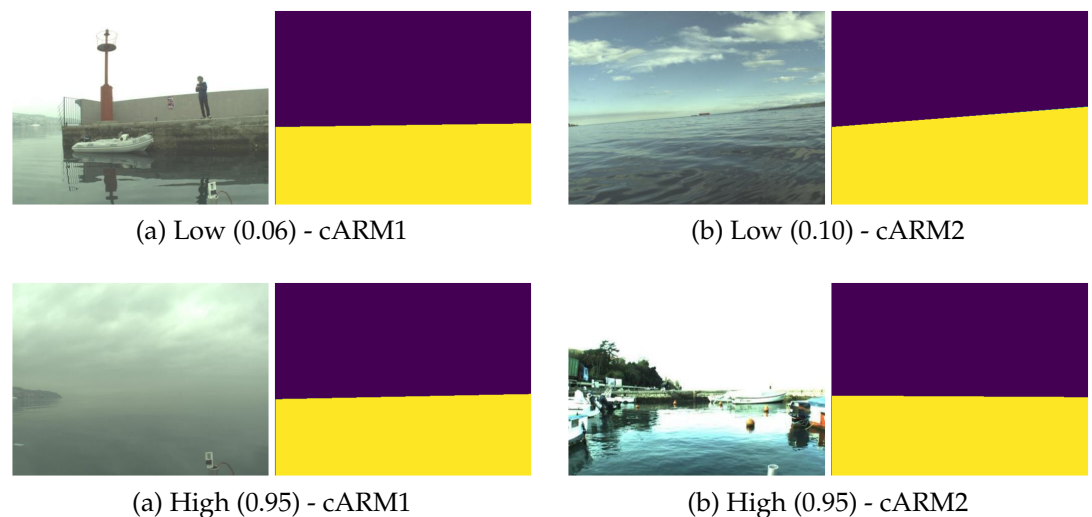


**Figure A1.** Example images and corresponding binary IMU masks for low (top row) and high (bottom row) weight prediction for IMU channel in cARM1 (left) and cARM2 (right) blocks. Weights (denoted in brackets) have higher values where the water edge is hardly visible due to bad weather conditions or extreme exposure.

## References

1. Bovcon, B.; Kristan, M. WaSR—A Water Segmentation and Refinement Maritime Obstacle Detection Network. *IEEE Transactions on Cybernetics* **2021**.

2. Žust, L.; Kristan, M. Temporal Context for Robust Maritime Obstacle Detection. In Proceedings of the 2022 IEEE/RSJ International Conference on Intelligent Robots and Systems (IROS), 2022.
3. Yao, L.; Kanoulas, D.; Ji, Z.; Liu, Y. ShorelineNet: an efficient deep learning approach for shoreline semantic segmentation for unmanned surface vehicles. In Proceedings of the 2021 IEEE/RSJ International Conference on Intelligent Robots and Systems (IROS). IEEE, 2021, pp. 5403–5409.
4. Ronneberger, O.; Fischer, P.; Brox, T. U-Net: Convolutional networks for biomedical image segmentation. In Proceedings of the International Conference on Medical image computing and computer-assisted intervention. Springer, 2015, pp. 234–241.
5. Chen, L.C.; Papandreou, G.; Kokkinos, I.; Murphy, K.; Yuille, A.L. DeepLab: Semantic Image Segmentation with Deep Convolutional Nets, Atrous Convolution, and Fully Connected CRFs. *IEEE transactions on pattern analysis and machine intelligence* **2017**, *40*, 834–848.
6. Google. Google Coral Edge TPU, 2021.
7. NVIDIA. Jetson Nano: A Powerful Low-Cost Platform for AI at the Edge, 2019.
8. Intel. Intel Movidius Myriad™ X Vision Processing Units, 2020.
9. Luxonis. OAK-D **2022**.
10. Steccanella, L.; Bloisi, D.D.; Castellini, A.; Farinelli, A. Waterline and obstacle detection in images from low-cost autonomous boats for environmental monitoring. *Robotics and Autonomous Systems* **2020**, *124*, 103346.
11. Howard, A.G.; Zhu, M.; Chen, B.; Kalenichenko, D.; Wang, W.; Weyand, T.; Andreetto, M.; Adam, H. Mobilenets: Efficient convolutional neural networks for mobile vision applications. *arXiv preprint arXiv:1704.04861* **2017**.
12. Sandler, M.; Howard, A.; Zhu, M.; Zhmoginov, A.; Chen, L.C. MobileNetV2: Inverted residuals and linear bottlenecks. In Proceedings of the Proceedings of the IEEE conference on computer vision and pattern recognition, 2018, pp. 4510–4520.
13. Han, K.; Wang, Y.; Tian, Q.; Guo, J.; Xu, C.; Xu, C. GhostNet: More features from cheap operations. In Proceedings of the Proceedings of the IEEE/CVF Conference on Computer Vision and Pattern Recognition, 2020, pp. 1580–1589.
14. Ma, N.; Zhang, X.; Zheng, H.T.; Sun, J. ShuffleNet V2: Practical guidelines for efficient cnn architecture design. In Proceedings of the Proceedings of the European conference on computer vision (ECCV), 2018, pp. 116–131.
15. Radosavovic, I.; Kosaraju, R.P.; Girshick, R.; He, K.; Dollár, P. Designing network design spaces. In Proceedings of the Proceedings of the IEEE/CVF conference on computer vision and pattern recognition, 2020, pp. 10428–10436.
16. Li, Y.; Chen, Y.; Dai, X.; Chen, D.; Liu, M.; Yuan, L.; Liu, Z.; Zhang, L.; Vasconcelos, N. MicroNet: Improving Image Recognition with Extremely Low FLOPs. In Proceedings of the Proceedings of the IEEE/CVF International Conference on Computer Vision, 2021, pp. 468–477.
17. Ding, X.; Zhang, X.; Ma, N.; Han, J.; Ding, G.; Sun, J. RepVGG: Making VGG-style Convnets Great Again. In Proceedings of the Proceedings of the IEEE/CVF Conference on Computer Vision and Pattern Recognition, 2021, pp. 13733–13742.
18. Vasu, P.K.A.; Gabriel, J.; Zhu, J.; Tuzel, O.; Ranjan, A. An Improved One millisecond Mobile Backbone. *arXiv preprint arXiv:2206.04040* **2022**.
19. Lee, J.M.; Lee, K.H.; Nam, B.; Wu, Y. Study on image-based ship detection for AR navigation. In Proceedings of the 2016 6th International Conference on IT Convergence and Security (ICITCS). IEEE, 2016, pp. 1–4.
20. Bloisi, D.D.; Previtali, F.; Pennisi, A.; Nardi, D.; Fiorini, M. Enhancing automatic maritime surveillance systems with visual information. *IEEE Transactions on Intelligent Transportation Systems* **2016**, *18*, 824–833.
21. Loomans, M.J.; de With, P.H.; Wijnhoven, R.G. Robust automatic ship tracking in harbours using active cameras. In Proceedings of the 2013 IEEE International Conference on Image Processing. IEEE, 2013, pp. 4117–4121.
22. Kristan, M.; Kenk, V.S.; Kovačič, S.; Perš, J. Fast image-based obstacle detection from unmanned surface vehicles. *IEEE transactions on cybernetics* **2015**, *46*, 641–654.
23. Prasad, D.K.; Prasath, C.K.; Rajan, D.; Rachmawati, L.; Rajabally, E.; Quek, C. Object detection in a maritime environment: Performance evaluation of background subtraction methods. *IEEE Transactions on Intelligent Transportation Systems* **2018**, *20*, 1787–1802.
24. Cane, T.; Ferryman, J. Saliency-based detection for maritime object tracking. In Proceedings of the Proceedings of the IEEE conference on computer vision and pattern recognition workshops, 2016, pp. 18–25.
25. Lee, S.J.; Roh, M.I.; Lee, H.W.; Ha, J.S.; Woo, I.G. Image-based ship detection and classification for unmanned surface vehicle using real-time object detection neural networks. In Proceedings of the The 28th International Ocean and Polar Engineering Conference. OnePetro, 2018.
26. Redmon, J.; Farhadi, A. YOLO9000: better, faster, stronger. In Proceedings of the Proceedings of the IEEE conference on computer vision and pattern recognition, 2017, pp. 7263–7271.
27. Prasad, D.K.; Rajan, D.; Rachmawati, L.; Rajabally, E.; Quek, C. Video processing from electro-optical sensors for object detection and tracking in a maritime environment: A survey. *IEEE Transactions on Intelligent Transportation Systems* **2017**, *18*, 1993–2016.
28. Yang, J.; Li, Y.; Zhang, Q.; Ren, Y. Surface vehicle detection and tracking with deep learning and appearance feature. In Proceedings of the 2019 5th International Conference on Control, Automation and Robotics (ICCAR). IEEE, 2019, pp. 276–280.
29. Ma, L.Y.; Xie, W.; Huang, H.B. Convolutional neural network based obstacle detection for unmanned surface vehicle. *Mathematical biosciences and engineering: MBE* **2019**, *17*, 845–861.

30. Ren, S.; He, K.; Girshick, R.; Sun, J. Faster R-CNN: Towards real-time object detection with region proposal networks. *Advances in neural information processing systems* **2015**, *28*.
31. He, K.; Zhang, X.; Ren, S.; Sun, J. Deep residual learning for image recognition. In Proceedings of the Proceedings of the IEEE conference on computer vision and pattern recognition, 2016, pp. 770–778.
32. Huang, G.; Liu, Z.; Van Der Maaten, L.; Weinberger, K.Q. Densely connected convolutional networks. In Proceedings of the Proceedings of the IEEE conference on computer vision and pattern recognition, 2017, pp. 4700–4708.
33. Cane, T.; Ferryman, J. Evaluating deep semantic segmentation networks for object detection in maritime surveillance. In Proceedings of the 2018 15th IEEE International Conference on Advanced Video and Signal Based Surveillance (AVSS). IEEE, 2018, pp. 1–6.
34. Badrinarayanan, V.; Kendall, A.; Cipolla, R. SegNet: A Deep Convolutional Encoder-Decoder Architecture for Image Segmentation. *IEEE transactions on pattern analysis and machine intelligence* **2017**, *39*, 2481–2495.
35. Paszke, A.; Chaurasia, A.; Kim, S.; Culurciello, E. ENet: A deep neural network architecture for real-time semantic segmentation. *arXiv preprint arXiv:1606.02147* **2016**.
36. Mehta, S.; Rastegari, M.; Caspi, A.; Shapiro, L.; Hajishirzi, H. ESPNet: Efficient spatial pyramid of dilated convolutions for semantic segmentation. In Proceedings of the Proceedings of the european conference on computer vision (ECCV), 2018, pp. 552–568.
37. Bovcon, B.; Muhovič, J.; Perš, J.; Kristan, M. The MaSTr1325 dataset for training deep USV obstacle detection models. In Proceedings of the 2019 IEEE/RSJ International Conference on Intelligent Robots and Systems (IROS). IEEE, 2019, pp. 3431–3438.
38. Zhao, H.; Shi, J.; Qi, X.; Wang, X.; Jia, J. Pyramid scene parsing network. In Proceedings of the Proceedings of the IEEE conference on computer vision and pattern recognition, 2017, pp. 2881–2890.
39. Yu, C.; Wang, J.; Peng, C.; Gao, C.; Yu, G.; Sang, N. BiSeNet: Bilateral Segmentation Network for Real-time Semantic Segmentation. In Proceedings of the Proceedings of the European conference on computer vision (ECCV), 2018, pp. 325–341.
40. Bovcon, B.; Muhovič, J.; Vranac, D.; Mozetič, D.; Perš, J.; Kristan, M. MODS—A USV-oriented object detection and obstacle segmentation benchmark. *IEEE Transactions on Intelligent Transportation Systems* **2021**.
41. Howard, A.; Sandler, M.; Chu, G.; Chen, L.C.; Chen, B.; Tan, M.; Wang, W.; Zhu, Y.; Pang, R.; Vasudevan, V.; et al. Searching for MobileNetV3. In Proceedings of the Proceedings of the IEEE/CVF International Conference on Computer Vision, 2019, pp. 1314–1324.
42. Hu, J.; Shen, L.; Sun, G. Squeeze-and-Excitation Networks. In Proceedings of the Proceedings of the IEEE conference on computer vision and pattern recognition, 2018, pp. 7132–7141.
43. Zhang, X.; Zhou, X.; Lin, M.; Sun, J. ShuffleNet: An extremely efficient convolutional neural network for mobile devices. In Proceedings of the Proceedings of the IEEE conference on computer vision and pattern recognition, 2018, pp. 6848–6856.
44. Tan, M.; Le, Q. EfficientNet: Rethinking model scaling for convolutional neural networks. In Proceedings of the International conference on machine learning. PMLR, 2019, pp. 6105–6114.
45. Tan, M.; Le, Q. EfficientNetV2: Smaller Models and Faster Training. In Proceedings of the International Conference on Machine Learning. PMLR, 2021, pp. 10096–10106.
46. Simonyan, K.; Zisserman, A. Very deep convolutional networks for large-scale image recognition. Computational and Biological Learning Society, 2015, pp. 1–14.
47. Yu, W.; Luo, M.; Zhou, P.; Si, C.; Zhou, Y.; Wang, X.; Feng, J.; Yan, S. MetaFormer is Actually What You Need for Vision. In Proceedings of the Proceedings of the IEEE/CVF Conference on Computer Vision and Pattern Recognition, 2022, pp. 10819–10829.
48. Zhao, H.; Qi, X.; Shen, X.; Shi, J.; Jia, J. ICNet for real-time semantic segmentation on high-resolution images. In Proceedings of the Proceedings of the European conference on computer vision (ECCV), 2018, pp. 405–420.
49. Wang, H.; Jiang, X.; Ren, H.; Hu, Y.; Bai, S. SwiftNet: Real-time video object segmentation. In Proceedings of the Proceedings of the IEEE/CVF Conference on Computer Vision and Pattern Recognition, 2021, pp. 1296–1305.
50. Zhang, W.; Huang, Z.; Luo, G.; Chen, T.; Wang, X.; Liu, W.; Yu, G.; Shen, C. TopFormer: Token Pyramid Transformer for Mobile Semantic Segmentation. In Proceedings of the Proceedings of the IEEE/CVF Conference on Computer Vision and Pattern Recognition, 2022, pp. 12083–12093.
51. Lin, T.Y.; Goyal, P.; Girshick, R.; He, K.; Dollár, P. Focal loss for dense object detection. In Proceedings of the Proceedings of the IEEE international conference on computer vision, 2017, pp. 2980–2988.
52. Vaswani, A.; Shazeer, N.; Parmar, N.; Uszkoreit, J.; Jones, L.; Gomez, A.N.; Kaiser, Ł.; Polosukhin, I. Attention is all you need. *Advances in neural information processing systems* **2017**, *30*.
53. Woo, S.; Park, J.; Lee, J.Y.; Kweon, I.S. Cbam: Convolutional block attention module. In Proceedings of the Proceedings of the European conference on computer vision (ECCV), 2018, pp. 3–19.
54. Krogh, A.; Hertz, J. A simple weight decay can improve generalization. *Advances in neural information processing systems* **1991**, *4*.
55. Popel, M.; Bojar, O. Training tips for the transformer model. *arXiv preprint arXiv:1804.00247* **2018**.
56. Carvalho, M.; Wightman, R.; Others. pytorch/vision, 2021. <https://doi.org/10.5281/zenodo.4779445>.
57. Yu, C.; Gao, C.; Wang, J.; Yu, G.; Shen, C.; Sang, N. BiSeNet V2: Bilateral Network with Guided Aggregation for Real-time Semantic Segmentation, 2020. <https://doi.org/10.48550/ARXIV.2004.02147>.

- 
58. Hong, Y.; Pan, H.; Sun, W.; Jia, Y. Deep Dual-resolution Networks for Real-time and Accurate Semantic Segmentation of Road Scenes. *arXiv preprint arXiv:2101.06085* **2021**.
  59. Pan, H.; Hong, Y.; Sun, W.; Jia, Y. Deep Dual-Resolution Networks for Real-Time and Accurate Semantic Segmentation of Traffic Scenes. *IEEE Transactions on Intelligent Transportation Systems* **2022**.
  60. Lo, S.Y.; Hang, H.M.; Chan, S.W.; Lin, J.J. Efficient dense modules of asymmetric convolution for real-time semantic segmentation. In *Proceedings of the ACM Multimedia Asia*; 2019; pp. 1–6.
  61. Lin, Z.Q.; Chwyl, B.; Wong, A. Edgesegnet: A compact network for semantic segmentation. *arXiv preprint arXiv:1905.04222* **2019**.
  62. Wang, Y.; Zhou, Q.; Liu, J.; Xiong, J.; Gao, G.; Wu, X.; Latecki, L.J. Lednet: A lightweight encoder-decoder network for real-time semantic segmentation. In *Proceedings of the 2019 IEEE International Conference on Image Processing (ICIP)*. IEEE, 2019, pp. 1860–1864.
  63. Jing, J.; Wang, Z.; Rättsch, M.; Zhang, H. Mobile-Unet: An efficient convolutional neural network for fabric defect detection. *Textile Research Journal* **2022**, *92*, 30–42.
  64. Gao, R. Rethink dilated convolution for real-time semantic segmentation. *arXiv preprint arXiv:2111.09957* **2021**.